Available online at www.sciencedirect.com

ScienceDirect

*Mendeleev Commun.*, 2023, **33**, 605–607

Mendeleev Communications

# Chemical bond in $FmO_2$

**Yury A. Teterin,*[a,b] Andrei E. Putkov,[a,b] Mikhail V. Ryzhkov,[c] Konstantin I. Maslakov,[a] Anton Yu. Teterin,[b] Kirill E. Ivanov,[b] Stepan N. Kalmykov[a] and Vladimir G. Petrov[a]**

[a] *Department of Chemistry, M. V. Lomonosov Moscow State University, 119991 Moscow, Russian Federation*
[b] *National Research Center 'Kurchatov Institute', 123182 Moscow, Russian Federation. E-mail: Teterin_YA@nrcki.ru*
[c] *Institute of Solid State Chemistry, Ural Branch of the Russian Academy of Sciences, 620990 Ekaterinburg, Russian Federation*

DOI: 10.1016/j.mencom.2023.09.004

**The density of electronic states and the XPS spectrum of $FmO_2$ valence electrons in the binding energy range from 0 to ~40 eV have been calculated by the fully relativistic method of discrete variation. It is shown that the electrons of the outer and inner valence molecular orbitals (MOs) with binding energies from 0 to ~15 eV and from ~15 to ~40 eV, respectively, contribute to the complex structure of the XPS spectrum of $FmO_2$. The $FmO_2$ MO diagram was constructed and the contribution of the electrons of the outer and inner valence MOs to the chemical bond was estimated.**

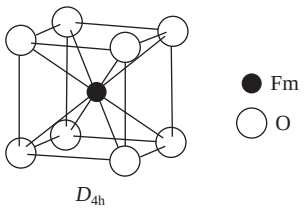


*Keywords*: $FmO_2$, chemical bond, electronic structure, XPS spectrum of valence electrons, relativistic method of discrete variation.

There are 19 known isotopes of fermium $_{100}$Fm.[1] The $^{255}$Fm isotope ($T_{1/2}$ = = 20.07 h, α-decay) is formed as a result of multiple capture of fast neutrons by $^{238}$U, followed by β-decay of the super-heavy uranium isotope. The $^{257}$Fm isotope ($T_{1/2}$ = 100.5 days, α-decay) can be obtained by neutron irradiation of plutonium in nuclear reactors. During the year, $10^9$ atoms of $^{257}$Fm are formed in reactors, which makes it possible to study this element.[1] The core level binding energies ($E_b$) of fermium were derived with an accuracy of ~10 eV from the data of conversion electron spectroscopy (β-decay $^{254m}$Es → $^{254}$Fm).[2,3] A $P_{2,3}$(Fm 6*p*) conversion electron spectrum was also observed at 24 ± 9 eV, but the surprisingly low energy was not explained.[2] Since it can be assumed that fermium is in the form of an oxide or other compounds, such a low Fm 6*p* binding energy compared to that known for $AnO_2$ oxides of light actinides[4,5] can be associated with the formation of outer valence molecular orbitals (OVMOs) ($E_b$ from 0 to ~15 eV) and inner valence molecular orbitals (IVMOs) ($E_b$ from ~15 to ~40 eV). To answer this question, relativistic calculations and X-ray photoelectron spectroscopy (XPS) data are required. Agreement with the experimental results will be a confirmation for the calculations.

Since the relativistic discrete variation (RDV) calculations of the valence XPS spectra of $AnO_2$ (An = Th, U–Bk) are in good agreement with the experimental data,[6] it can be assumed that the calculated valence XPS spectrum of $FmO_2$ can reflect the real experimental spectrum. This will make it possible to reveal the general regularities in the formation of a complex valence XPS structure in $AnO_2$ (An = Th–Lr) and the features of the nature of the chemical bond in these oxides.

To determine the density of electronic states and simulate the valence XPS spectrum, as well as to elucidate the nature of the chemical bond in $FmO_2$, a fully relativistic RDV calculation of the electronic structure of this oxide was carried out.

The cluster $FmO_8^{12-}$ (symmetry group $D_{4h}$), reflecting the close environment of fermium in $FmO_2$, is a body-centered cube with fermium in the center, surrounded by eight oxygen atoms at the vertices with an interatomic distance $R_{Fm–O}$ = 0.2279 nm, obtained by extrapolation of known experimental values of $R_{An–O}$ (An = Th–Es).[6]

For the first time, calculations of the electronic structure were carried out in the self-consistent field RDV approximation[7,8] based on the solution of the Dirac–Slater equation for four-component spinors with an exchange-correlation potential.[9] The extended basis of numerical atomic orbitals (AOs) obtained as a solution of the Dirac–Slater equation for isolated neutral atoms also included the Fm $6d_{3/2}$, $6d_{5/2}$, $7p_{1/2}$, $7p_{3/2}$ functions in addition to the occupied AOs. Besides, this basis took into account cluster symmetry, *i.e.*, the technique of projection operators[7] constructed AO linear combinations transformed by irreducible representations of the double group $D_{4h}$. To obtain relativistic bases, an original symmetrization program was employed, using matrices of irreducible representations for most of the double groups considered earlier[9,10] and transformation matrices.[11] Numerical Diophantine integration in the calculation of matrix elements was carried out for 22 000 sample points distributed in the cluster space. This ensured the convergence of valence molecular orbital (MO) energies better than 0.1 eV. The absence of any muffin-tin approximation in the RDV method is an advantage, since it does not impose restrictions on the symmetry of the compounds under study. Any types of clusters (including those without symmetry) can be calculated with the same accuracy. Also, calculations in the MO LCAO (molecular orbitals as linear combinations of atomic orbitals) approximation make it possible to estimate the role of atomic states in the electronic structure, chemical bond, spectral and other properties of solid compounds.

The ground state valence electron configuration of fermium is Fm $6s^26p^65f^{12}6d^07s^27p^0$, $^3H_6$. These electron shells can be involved

in MO formation in $FmO_2$.[4,5] MO compositions and energies in $FmO_2$ calculated by the RDV method are given in Table S1 (see Online Supplementary Materials).

The valence MOs also include the Fm 6*d* and 7*p* AOs, which are vacant in the atomic Fm. The Fm 6*p*, 6*d* and 5*f* AOs make the greatest contribution to the formation of MOs, the Fm 7*s* and 7*p* AOs make a smaller contribution to the formation of MOs, and the Fm 6*s* AO does not participate in the formation of MOs (Figure 1).

The upper filled $22\gamma_7^-$ and $25\gamma_6^-$ OVMOs consist of 71% Fm 5*f* AOs or 2.84 5*f* electrons (see Figure 1, labeled *1*). Such Fm 5*f* electrons can formally be considered 'localized' around the Fermi level. The remaining Fm 5*f* electrons are delocalized mainly in the OVMO range. The significant participation of Fm 5*f*, 6*d* and O 2*p* AOs in the formation of OVMOs is consistent with the results for $AnO_2$ of light actinides.[6] At the same time, the contribution of the Fm 5*f* AO to the O 2*s*-type MO remains insignificant.

The composition of OVMOs with the participation of Fm 6*d*, 7*s* and 7*p* AOs in $FmO_2$ does not change significantly in comparison with the dioxides of light actinides.[6] These orbitals, together with the O 2*s* and O 2*p* AOs, form a 'rigid frame' containing the An 5*f* MOs.

The Fm 6*p* AOs in $FmO_2$ are involved in MO formation, as well as An 6*p* in light actinide dioxides. As a result, 'antibonding' IVMOs $17\gamma_6^-$, $13\gamma_7^-$ (labeled *5*) and $16\gamma_6^-$ (labeled *7*) and 'bonding' IVMOs $15\gamma_6^-$, $11\gamma_7^-$ (labeled *8*) and $14\gamma_6^-$ (labeled *9*) formally appear (see Figure 1). However, in this case, the Fm $6p_{3/2}$ and O 2*s* AOs practically overlap (see Table S1).

Significant covalence effects in $FmO_2$ are observed due to significant overlap in the Fm 5*f*–O 2*p* and Fm 6*d*–O 2*p* AO pairs.

Due to the covalence of the Fm–O overlap, the effective charge of Fm ($Q_{Fm}$, in electrons) in $FmO_2$ differs from that in the ionic approximation Fm $6s^26p^65f^{10}6d^07s^0$ ($Q_{Fm}$ = +4 electrons). In this case, the effective charge is the difference between the charges calculated by the RDV method for the configurations, Fm $6s^26p^65f^{11.44}6d^{1.32}7s^{0.24}7p^{0.58}$ for $FmO_2$ and the valence atomic Fm $6s^26p^65f^{12}6d^07s^27p^0$. This value ($Q_{Fm}$ = +0.42 electrons) is significantly lower than that calculated in the ionic approximation ($Q_{Fm}$ = +4 electrons). These results are in qualitative agreement with data for other actinide dioxides.[12,13] Such a low effective charge in $FmO_2$ is also consistent with XPS data on chemical shifts (several eV) of actinide peaks between metallic actinides and dioxides.[5] The effective charge $Q_{Fm}$ = +4 electrons would result in a shift of dozens of eV. It is known that a vacancy at the quasi-atomic level (*e.g.*, Ce 3*d* in $CeO_2$) leads to a shift of ~16.0 eV.[14]

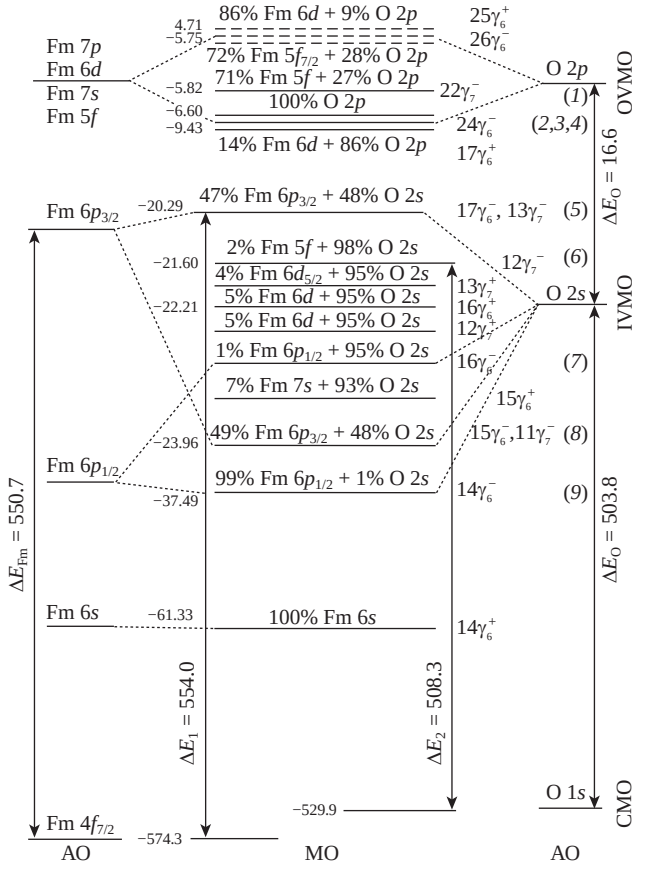


**Figure 1** MO diagram of the $FmO_8$ cluster, built according to theoretical data. Chemical shifts during cluster formation are not indicated. Arrows show some measurable differences in binding energy levels. The experimental binding energies (eV) are given on the left. Energy is not scaled.

The experimental valence and core XPS data, as well as the results of calculations,[6] were used to construct MO diagrams for light actinide dioxides. As a result, quantitative, energy-normalized theoretical and experimental spectra were obtained. These spectra could be considered in a unified energy scale. In this scale, the $E_b$ values for the $12\gamma_7^-$ IVMO and the O 1*s* AO are 21.60 and 529.9 eV, respectively.[15] This made it possible to compare the theoretical and experimental valence XPS spectra of the actinide series dioxides.

When constructing the MO diagram for $FmO_2$, the Fm $4f_{7/2}$ binding energy $E_b$(Fm $4f_{7/2}$) = 574.3 ± 0.4 eV and the spin–orbit splitting $\Delta E_{sl}$(Fm $4f_{7/2}$) = 18.6 ± 0.3 eV were taken into account. These values were obtained by extrapolating known experimental values for $AnO_2$ (An = Th, U–Bk) using the equations:[15]

$$E_b(\text{An } 4f_{7/2}) = 0.21255Z^2 - 16.43351Z + 92.16 \quad (R^2 = 0.99991), \quad (1)$$

$$\Delta E_{sl}(\text{An } 4f) = 0.95Z - 76.425 \quad (R^2 = 0.99285), \quad (2)$$

where $E_b$(An $4f_{7/2}$) is the An $4f_{7/2}$ binding energy, $\Delta E_{sl}$(An 4*f*) is the spin–orbit splitting equal to the difference between the binding energies for An $4f_{5/2}$ and An $4f_{7/2}$, *Z* is the atomic number of the actinide and *R* is the correlation coefficient.

The obtained values of $E_b$(Fm $4f_{7/2}$) and $\Delta E_{sl}$(Fm 4*f*) are the most accurate among all the earlier values[16] and agree satisfactorily with the results of relativistic calculations of the electronic structure of $FmO_2$ (see Figure 1).

Vacant and filled MOs in the $FmO_2$ MO diagram are shown by dashed and solid lines, respectively (see Figure 1). The calculated binding energies of the valence MOs are shown to the left of the MOs. The MO compositions in percent are shown above the MO lines. The MO designations are on the right, and the MO group labels are given in parentheses to simplify the discussion of the MO diagram. The vertical arrows show the experimentally measured differences in the binding energies between the core MOs (CMOs) and valence MOs; the values of the $E_b$ differences are shown on the left. The value of $\Delta E_{Fm}^T$ (energy difference between the Fm $6p_{3/2}$ and Fm $4f_{7/2}$ levels) is 550.73 eV.[17]

On the MO diagram (see Figure 1), one can formally distinguish the 'antibonding' $17\gamma_6^-$, $13\gamma_7^-$ (labeled *5*) and $16\gamma_6^-$ (labeled *7*) IVMOs and the corresponding 'bonding' $15\gamma_6^-$, $11\gamma_7^-$ (labeled *8*) and $14\gamma_6^-$ (labeled *9*) IVMOs, as well as the 'quasi-atomic' $12\gamma_7^-$, $13\gamma_7^+$, $12\gamma_7^+$, $16\gamma_6^+$ and $15\gamma_6^+$ (labeled *6*) IVMOs, formed mainly from the O 2*s* AOs. The MO diagram allows one to understand the nature of the chemical bond in $FmO_2$.

To evaluate the contribution of different MOs to the chemical bond in $FmO_2$, in this work, we performed RDV calculations of the overlapping populations of MOs in the Mulliken approximation[12,18] (Table 1). Positive populations indicate strengthening of the bond (bonding), negative values indicate weakening of the bond (antibonding).

The contribution to the bond population in $FmO_2$, including OVMOs, is 357 units (see Table 1). The greatest contribution to bond strengthening is made by the electrons of the Fm 6*d*–O 2*p*, Fm 7*p*–O 2*p*, Fm 6*d*–O 2*s* and Fm 5*f*–O 2*p* MOs with population

**Table 1** Overlapping populations of MOs in $FmO_2$ (per ligand, $\times10^3$) by RDV.

| OVMOs | | | | IVMOs | |
|---|---|---|---|---|---|
| MO in $FmO_2$ | RDV value | MO in $FmO_2$ | RDV value | MO in $FmO_2$ | RDV value |
| Fm 5$f_{5/2}$–O 2$p$ | −4 | Fm 7$p_{3/2}$–O 2$s$ | 9 | Fm 6$p_{1/2}$–O 2$p$ | −11 |
| Fm 5$f_{7/2}$–O 2$p$ | 23 | Fm 7$s$–O 2$p$ | 23 | Fm 6$p_{3/2}$–O 2$p$ | −66 |
| Fm 5$f_{5/2}$–O 2$s$ | −3 | Fm 7$s$–O 2$s$ | 20 | Fm 6$p_{1/2}$–O 2$s$ | −2 |
| Fm 5$f_{7/2}$–O 2$s$ | 2 | Fm 6$d_{3/2}$–O 2$p$ | 68 | Fm 6$p_{3/2}$–O 2$s$ | −22 |
| Fm 7$p_{1/2}$–O 2$p$ | 21 | Fm 6$d_{5/2}$–O 2$p$ | 98 | Fm 6$s$–O 2$p$ | −16 |
| Fm 7$p_{3/2}$–O 2$p$ | 46 | Fm 6$d_{3/2}$–O 2$s$ | 16 | Fm 6$s$–O 2$s$ | −1 |
| Fm 7$p_{1/2}$–O 2$s$ | 12 | Fm 6$d_{5/2}$–O 2$s$ | 26 | | |
| $\Sigma_{OVMO}$[a] | | | 357 | $\Sigma_{IVMO}$[a] | −118 |
| $\Sigma_{MO}$[a] | | | | | 239 |

[a] OVMO, IVMO and MO contributions.

values of 166, 67, 42 and 19 units, respectively. Inner valence electrons weaken the bond in $FmO_2$, while their total contribution is −118 units. The largest antibonding contribution, estimated at −77 units, is made by the electrons of the Fm 6$p$–O 2$p$ MO. Together, the IVMO electrons (−118 units) weaken the bond strengthened by the OVMO electrons (357 units) by 33%. As a result, the total contribution of valence electrons to the chemical bond in $FmO_2$ is 239 units of overlapping populations.

Experimental core and valence XPS spectra of fermium dioxide are currently absent. The calculation of the valence XPS structure of $FmO_2$ is based on the data of a relativistic calculation of the density of electronic states with allowance for photoemission cross-sections.

To compare the valence XPS structure of the $FmO_2$ with the corresponding data for light actinides, the calculated MO energies were increased in absolute value by 5.82 eV, so that the $12\gamma_7^-$ IVMO energy (labeled *6*) became 21.6 eV. Taking into account the MO compositions (see Table S1) and the photoemission cross-sections, the peak intensities of the $FmO_2$ valence XPS spectrum were calculated (Figure 2).

The XPS spectrum of $FmO_2$, calculated in the range of binding energies from 0 to ~40 eV, can be subdivided into two ranges (see Figure 2). In the first range from 0 to ~15 eV, a structure associated with the OVMO electrons is observed. The intensity of this band mainly depends on the Fm 5$f$ and Fm 6$d$ electrons, since their photoemission cross-sections are much higher than those of the Fm 7$s$, Fm 7$p$ and O 2$p$ electrons.

The second range, from ~15 to ~40 eV, has a structure associated with the IVMO electrons due to the strong Fm 6$p_{3/2}$–O 2$s$ AO overlapping. This range can be subdivided into five components (labeled *5*–*9*): 'antibonding' IVMOs $17\gamma_6^-$ and $13\gamma_7^-$ (labeled *5*); IVMOs $12\gamma_7^-$ (labeled *6*), $13\gamma_7^+$, $12\gamma_7^+$, $16\gamma_6^+$ and $15\gamma_6^+$ containing the quasi-atomic O 2$s$ AOs; formally 'antibonding' IVMO $16\gamma_6^-$ (labeled *7*); 'bonding' IVMOs $15\gamma_6^-$ and $11\gamma_7^-$ (labeled *8*); and formally 'bonding' IVMO $14\gamma_6^-$ (labeled *9*).

The results of this calculation make it possible to quantitatively understand the features of the nature of the chemical bond and the structure of the valence XPS spectrum of $FmO_2$ in the binding energy range from 0 to ~40 eV (see Figure 2).

Thus, on the basis of the fully relativistic calculation of the electronic structure of $FmO_2$, the valence electronic density of states was determined. The theoretical valence XPS spectrum in the binding energy range from 0 to ~40 eV was constructed and analyzed taking into account experimental XPS data for the core and valence electrons of $AnO_2$ (An = Th–Es) dioxides. The MO

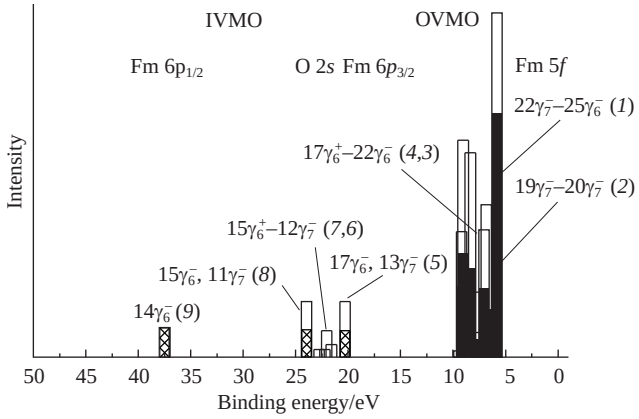


**Figure 2** Histogram of the $FmO_2$ valence XPS spectrum calculated by the RDV method. The contributions of the Fm 5$f$ and Fm 6$p$ AOs to the (*1*)–(*4*) OVMOs and (*5*)–(*9*) IVMOs are indicated by solid and cross-shaped fill, respectively.

diagram for $FmO_2$ was built. This diagram makes it possible to understand the XPS structure and the nature of the chemical bond in $FmO_2$ and to reveal the general regularities and features of the formation of a chemical bond in the $AnO_2$ (An = Th–Lr) dioxide series.

*Online Supplementary Materials*

Supplementary data associated with this article can be found in the online version at doi: 10.1016/j.mencom.2023.09.004.

## References

1 *The Chemistry of the Actinide and Transactinide Elements*, 4th edn., eds. L. R. Morss, N. M. Edelstein and J. Fuger, Springer, Dordrecht, 2010.
2 F. T. Porter and M. S. Freedman, *Phys. Rev. Lett.*, 1971, **27**, 293.
3 M. O. Krause and C. W. Nestor, Jr., *Phys. Scr.*, 1977, **16**, 285.
4 Y. A. Teterin and S. G. Gagarin, *Russ. Chem. Rev.*, 1996, **65**, 825 (*Usp. Khim.*, 1996, **65**, 825).
5 Y. A. Teterin and A. Y. Teterin, *Russ. Chem. Rev.*, 2004, **73**, 541 (*Usp. Khim.*, 2004, **73**, 588).
6 A. E. Putkov, Yu. A. Teterin, M. V. Ryzhkov, A. Yu. Teterin, K. I. Maslakov, K. E. Ivanov, S. N. Kalmykov and V. G. Petrov, *Russ. J. Phys. Chem. A*, 2021, **95**, 1169 (*Zh. Fiz. Khim.*, 2021, **95**, 908).
7 A. Rosen and D. E. Ellis, *J. Chem. Phys.*, 1975, **62**, 3039.
8 D. E. Ellis and G. L. Goodman, *Int. J. Quantum Chem.*, 1984, **25**, 185.
9 O. Gunnarsson and B. I. Lundqvist, *Phys. Rev. B: Solid State*, 1976, **13**, 4274.
10 P. Pyykkö and H. Toivonen, *Acta Acad. Abo., Ser. B*, 1983, **43** (2), 1.
11 D. A. Varshalovish, A. N. Moskalev and V. K. Khersonskii, *Quantum Theory of Angular Momentum*, World Scientific, Singapore, 1988.
12 P. J. Kelly, M. S. S. Brooks and R. Allen, *J. Phys., Colloq.*, 1979, **40** (C4), 184.
13 V. A. Gubanov, A. Rosén and D. E. Ellis, *J. Phys. Chem. Solids*, 1979, **40**, 17.
14 K. I. Maslakov, Y. A. Teterin, M. V. Ryzhkov, A. J. Popel, A. Y. Teterin, K. E. Ivanov, S. N. Kalmykov, V. G. Petrov, P. K. Petrov and I. Farnan, *Phys. Chem. Chem. Phys.*, 2018, **20**, 16167.
15 Yu. A. Teterin, M. V. Ryzhkov, A. E. Putkov, K. I. Maslakov, A. Yu. Teterin, K. E. Ivanov, S. N. Kalmykov and V. G. Petrov, *Russ. J. Inorg. Chem.*, 2022, **67**, 881 (*Zh. Neorg. Khim.*, 2022, **67**, 817).
16 K. D. Sevier, *At. Data Nucl. Data Tables*, 1979, **24**, 323.
17 K.-N. Huang, M. Aoyagi, M. H. Chen, B. Crasemann and H. Mark, *At. Data Nucl. Data Tables*, 1976, **18**, 243.
18 R. S. Mulliken, *Annu. Rev. Phys. Chem.*, 1978, **29**, 1.

*Received: 15th May 2023; Com. 23/7170*